differences in the conception sex ratio related to individual phenotypic variation may require favourable environmental conditions, whereas differences in the susceptibility of male and female fetuses to nutritional stress may generate population-wide trends in annual birth sex ratios. In the Rum red deer population, the action of one mechanism swamped the other within about two generations. This may explain why general trends in sex-ratio variation have been so difficult to detect. □

Methods

Since 1971, life history data have been collected on individual red deer (*Cervus elaphus*) in the North Block of the Isle of Rum, Scotland, an area of about 12 km^2 (ref. 18). We take as our measure of density the number of females of more than one year old in the study area; since the cessation of culling in 1973, density has risen from 57 to 178. Females produce at most one calf per year throughout their breeding lifespan, whereas male reproductive success shows greater variance; adult male weight is 1.7 times that of females, and male calves are heavier at birth[18]. All animals in the study population are individually recognizable; daily monitoring of the population during the calving season shows whether or not each female calved in a given year, and, if so, the sex of her offspring. An age-corrected dominance rank for each female, ranging from 0 to 1, is calculated from observations of interactions between pairs of individuals, as described elsewhere.[2] Females are also classified as to whether or not they reared a calf the previous year that survived to six months. Average temperature and total rainfall in the following periods were considered: August to October, November to January, February to March. None of the weather variables showed consistent change over the study period.

We report two forms of statistical analysis. The proportion of males born each year (referred to as the annual birth sex ratio) was related to density and weather measures using simple linear regression (normality of errors was satisfied; 1973 was excluded owing to incomplete data collection). The probability that an individual calf was male and the probability that a female gave birth in a given year were analysed using generalized linear mixed models[28], with restricted maximum likelihood estimation of variance components. Just as generalized linear models allow the extension of general linear models to data where the errors are not normally distributed, GLMMs allow similar extensions to the conventional mixed model case where the response variable is determined by both random and fixed effects. In this case, the random component arose because of repeated sampling within a year and repeated sampling of the same females across years. Year and female identity were therefore fitted as random effects. In both models, the response variables were binary (male, not male; had calf, did not have calf), necessitating the use of a logit link function. The significance of the explanatory terms, the fixed effects, was assessed by their Wald statistics (distributed as χ^2) for each term when fitted last in the model. All interaction terms were tested, but are not reported unless statistically significant. Analysis was performed in Genstat 5, version 3.2.

Received 26 January; accepted 26 March 1999.

1. Clutton-Brock, T. H. & Iason, G. R. Sex ratio variation in mammals. *Q. Rev. Biol.* **61,** 339–373 (1986).
2. Clutton-Brock, T. H., Albon, S. D. & Guinness, F. E. Great expectations: dominance, breeding success and offspring sex ratios in red deer. *Anim. Behav.* **34,** 460–471 (1986).
3. Clutton-Brock, T. H., Albon, S. D. & Guinness, F. E. Maternal dominance, breeding success and birth sex ratios in red deer. *Nature* **308,** 358–360 (1984).
4. Trivers, R. L. & Willard, D. E. Natural selection of parental ability to vary the sex ratio of offspring. *Science* **179,** 90–92 (1973).
5. Hiraiwa-Hasegawa, M. Skewed birth sex ratios in primates: should high-ranking mothers have daughters or sons? *Trends Ecol. Evol.* **8,** 395–399 (1993).
6. Cassinello, J. High-ranking females bias their investment in favour of male calves in captive *Ammotragus iervia*. *Behav. Ecol. Sociobiol.* **38,** 417–424 (1996).
7. Meikle, D. B., Drickamer, L. C., Bessey, S. H., Arthur, R. D. & Rosenthal, T. L. Dominance rank and parental investment in swine (*Sus scrofa domesticus*). *Ethology* **102,** 969–978 (1996).
8. Kojola, I. & Eloranta, E. Influences of maternal body weight, age, and parity on sex ratio in semidomesticated reindeer (*Rangifer t. tarandus*). *Evolution* **43,** 1331–1336 (1989).
9. Rutberg, A. T. Lactation and fetal sex ratios in American bison. *Am. Nat.* **127,** 89–94 (1986).
10. Wauters, L. A., Decrombrugghe, S. A., Nour, N. & Matthysen, E. Do female roe deer in good condition produce more sons than daughters? *Behav. Ecol. Sociobiol.* **37,** 189–193 (1995).
11. Flint, A. P. F., Albon, S. D. & Jafar, S. I. Blastocyst development and conceptus sex selection in red deer *Cervus elaphus*: studies of a free-living population on the Isle of Rum. *Gen. Comp. Endocrinol.* **106** 374–383 (1997).
12. Mendl, M., Zenlla, A. J., Broom, D. M. & Whittemore, C. T. Maternal social-status and birth sex-ratio in domestic pigs: an analysis of mechanisms. *Ethol. Sociobiol.* **16,** 257–333 (1995).
13. Nygren, T. & Kojola, I. Twinning and fetal sex ratio in moose: effects of maternal age and mass. *Can. J. Zool.* **75,** 1945–1948 (1997).
14. Birgersson, B. Adaptive adjustment of the sex ratio: more data and considerations from a fallow deer population. *Behav. Ecol.* **9,** 404–408 (1998).
15. Hewison, A. J. M. & Gaillard, J. M. Birth-sex ratios and local resource competition in roe deer, *Capreolus capreolus*. *Behav. Ecol.* **7,** 461–464 (1996).
16. Festa-Bianchet, M. The social system of bighorn sheep: grouping patterns, kinship and female dominance rank. *Anim. Behav.* **42,** 71–82 (1991).
17. Albon, S. D., Coulson, T. N. & Clutton-Brock, T. H. in *Recent Developments in Deer Biology* (ed. Milne, J. A.) 85–95 (Macaulay Land Use Research Institute, Craigiebuckler, Aberdeen and Moredun Research Institute, Edinburgh, 1998).
18. Clutton-Brock, T. H., Guinness, F. E. & Albon, S. D. *Red Deer—Behaviour and Ecology of Two Sexes* (University of Chicago Press, Chicago, 1982).
19. Gomendio, M., Clutton-Brock, T. H., Albon, S. D., Guinness, F. E. & Simpson, M. J. Mammalian sex ratios and variation in costs of rearing sons and daughters. *Nature* **343,** 261–263 (1990).
20. Flint, A. P. F., Albon, S. D., Loudon, A. S. I. & Jabbour, H. N. Behavioral dominance and corpus luteum function in red deer *Cervus elaphus*. *Horm. Behav.* **31,** 296–304 (1997).
21. Albon, S. D., Clutton-Brock, T. H. & Guinness, F. E. Early development and population dynamics in red deer II. Density-independent effects and cohort variation. *J. Anim. Ecol.* **56,** 69–81 (1987).
22. Coulson, T. N., Albon, S. D., Slate, J. & Pemberton, J. M. Sex dependent responses to inbreeding and outbreeding in red deer calves. *Evolution* (in the press).
23. Clutton-Brock, T. H., Albon, S. D. & Guinness, F. E. Parental investment and sex differences in juvenile mortality in birds and mammals. *Nature* **313,** 131–133 (1985).
24. Kent, J. P. Birth sex ratios in sheep over nine lambing seasons: years 7–9 and the effects of ageing. *Behav. Ecol. Sociobiol.* **36,** 101–104 (1995).
25. Byers, J. A. *American Pronghorn: Social Adaptations and the Ghosts of Predators Past* (Univ. of Chicago Press, Chicago, 1997).
26. Green, W. C. H. & Rothstein, A. Sex bias or equal opportunity—patterns of maternal investment in bison. *Behav. Ecol. Sociobiol.* **29,** 373–384 (1991).
27. Lloyd, P. H. & Rasa, O. A. E. Status, reproductive success and fitness in Cape mountain zebra (*Equus zebra zebra*). *Behav. Ecol. Sociobiol.* **25,** 411–420 (1989).
28. Schall, R. Estimation in generalized linear models with random effects. *Biometrika* **78,** 719–727 (1991).

Acknowledgements. We thank Scottish Natural Heritage for permission to work on Rum; their local staff for help and support; A. Alexander, A. Curnow, S. Morris and many others for field data collection; N. Barton, P. Brotherton, A. Cockburn, D. Elston, M. Forchhammer, H. Kruuk, J. Lindström, A. Manning and P. Meir for comments and discussion; and the NERC for funding this work.

Correspondence and requests for materials should be addressed to L.K. (e-mail: Loeske.Kruuk@ed.ac.uk).

Multifractality in human heartbeat dynamics

Plamen Ch. Ivanov*†, Luís A. Nunes Amaral*†, Ary L. Goldberger†, Shlomo Havlin‡, Michael G. Rosenblum§, Zbigniew R. Struzik‖ & H. Eugene Stanley*

** Center for Polymer Studies and Department of Physics, Boston University, Boston, Massachusetts 02215, USA*
† Harvard Medical School, Beth Israel Deaconess Medical Center, Boston, Massachusetts 02215, USA
‡ Gonda Goldschmid Center and Department of Physics, Bar-Ilan University, Ramat Gan, Israel
§ Department of Physics, Potsdam University, 14415 Potsdam, Germany
‖ Centre for Mathematical and Computing Science, Kruislaan 413, NL-1098 SJ Amsterdam, The Netherlands

There is evidence that physiological signals under healthy conditions may have a fractal temporal structure[1]. Here we investigate the possibility that time series generated by certain physiological control systems may be members of a special class of complex processes, termed multifractal, which require a large number of exponents to characterize their scaling properties[2–6]. We report on evidence for multifractality in a biological dynamical system, the healthy human heartbeat, and show that the multifractal character and nonlinear properties of the healthy heart rate are encoded in the Fourier phases. We uncover a loss of multifractality for a life-threatening condition, congestive heart failure.

Biomedical signals are generated by complex self-regulating systems that process inputs with a broad range of characteristics[7,8]. Many physiological time series, such as the one shown in Fig. 1a, are extremely inhomogeneous and non-stationary, fluctuating in an irregular and complex manner. The analysis of the fractal properties of such fluctuations has been restricted to second-order linear characteristics such as the power spectrum and the two-point autocorrelation function. These analyses reveal that the fractal behaviour of healthy, free-running physiological systems is often

characterized by $1/f$-like scaling of the power spectra, $S(f)$, where f is the frequency[9–12].

Monofractal signals are homogeneous, in the sense that they have the same scaling properties throughout the entire signal. Therefore, monofractal signals can be indexed by a single global exponent—the Hurst exponent H (ref. 13). Multifractal signals, on the other hand, can be decomposed into many subsets characterized by different local Hurst exponents h, which quantify the local singular behaviour and thus relate to the local scaling of the time series. Thus, multifractal signals require many exponents to characterize their scaling properties fully[4–6].

The statistical properties of the different subsets characterized by these different exponents h can be quantified by the function $D(h)$, where $D(h_0)$ is the fractal dimension of the subset of the time series characterized by the local Hurst exponent h_0[2,4–6]. Thus, the multifractal approach for signals, a concept introduced in the context of multi-affine functions[14,15], has the potential to describe a wide class of signals that are more complex than those characterized by a single fractal dimension (such as classical $1/f$ noise).

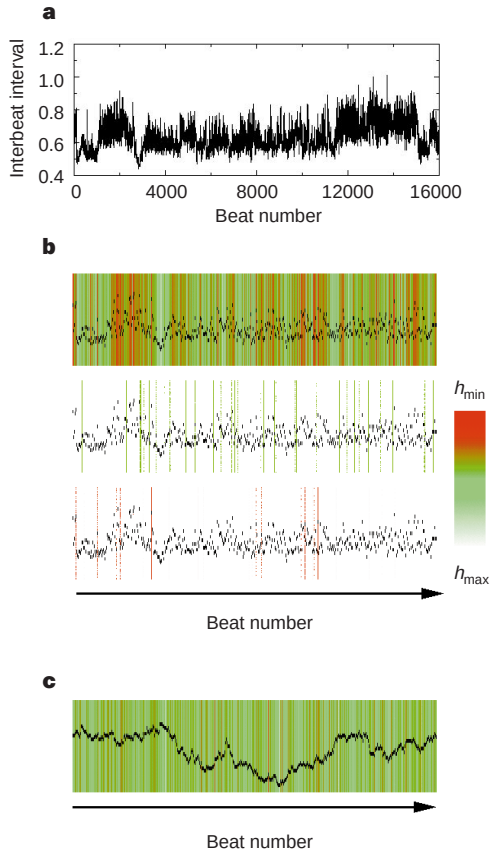

Figure 1 Visualization of multifractality in the hearbeat. **a**, Consecutive heartbeat intervals (in s) versus beat number for ~3 h data from a representative healthy subject. The time series exhibits very irregular and nonstationary behaviour. **b**, Top, the local Hurst exponents calculated for the 3 h record shown in **a**. The heterogeneity of the healthy heartbeat is represented by the broad range of local Hurst exponents h (colours) present and the complex temporal organization of the different exponents. Middle and bottom, the different fractal structures of two subsets of the time series characterized by different local Hurst exponents. The value of the local Hurst exponent for each subset is represented with a shade of green and red, respectively. The two subsets display different temporal structures which can be quantified by different fractal dimensions $D(h)$. **c**, The local Hurst exponents calculated for a monofractal signal–fractional Brownian motion with $H = 0.6$. The homogeneity of the signal is represented by the nearly monochromatic appearance of the signal which indicates that the local Hurst exponent h is the same throughout the signal and identical to the global Hurst exponent H.

We tested whether a large number of exponents is required to characterize heterogeneous heartbeat interval time series (Fig. 1) by undertaking multifractal analysis. The first problem is to extract the local value of h. To this end, we used methods derived from wavelet theory[16]. The properties of the wavelet transform make wavelet methods attractive for the analysis of complex non-stationary time series such as those found in physiological systems[17]. In particular, wavelets can remove polynomial trends that could cause box-counting techniques to fail to quantify the local scaling of the signal[18]. Additionally, the time-frequency localization properties of wavelets makes them particularly useful for revealing the underlying hierarchy that governs the temporal distribution of the local Hurst exponents[19]. Thus, the wavelet transform allows a reliable multifractal analysis to be performed[18,19]. We used derivatives of the gaussian function as the analysing wavelet, which allowed us to estimate the singular behaviour and the corresponding exponent h at a given location in the time series. The higher the order, n, of the derivative, the higher the order of the polynomial trends removed and the better the detection of the temporal structure of the local scaling exponents in the signal.

We evaluated the local exponent h through the modulus of the maxima values of the wavelet transform at each point in the time series. We then estimated the scaling of the partition function $Z_q(a)$, which is defined as the sum of the qth powers of the local maxima of the modulus of the wavelet transform coefficients at scale a (ref. 19). For small scales, we expect

$$Z_q(a) \simeq a^{\tau(q)}. \quad (1)$$

For certain values of q, the exponents $\tau(q)$ have familiar meanings. In particular, $\tau(2)$ is related to the scaling exponent of the Fourier power spectra, $S(f) \sim 1/f^{\beta}$, as $\beta = 2 + \tau(2)$. For positive q, $Z_q(a)$ reflects the scaling of the large fluctuations and strong singularities, whereas for negative q, $Z_q(a)$ reflects the scaling of the small fluctuations and weak singularities[4,5]. Thus, the scaling exponents $\tau(q)$ can reveal different aspects of cardiac dynamics.

Monofractal signals display a linear $\tau(q)$ spectrum, $\tau(q) = qH - 1$, where H is the global Hurst exponent. For multifractal signals, $\tau(q)$ is a nonlinear function: $\tau(q) = qh - D(b)$, where $h = \mathrm{d}\tau/\mathrm{d}q$ is not constant. The fractal dimension $D(h)$, introduced earlier, is related to $\tau(q)$ through a Legendre transform:

$$D(h) = qh - \tau(q). \quad (2)$$

We analysed both daytime (12:00 to 18:00) and night-time (0:00 to 6:00) heartbeat time series records from healthy subjects, and the daytime records of patients with congestive heart failure. These data were obtained by Holter monitoring[20]. Our database includes 18 healthy subjects (13 female and 5 male, with ages between 20 and 50, average 34.3 years), and 12 congestive heart failure subjects (3 female and 9 male, with ages between 22 and 71, average 60.8 years) in sinus rhythm (see Methods for details on data acquisition and preprocessing). For all subjects, for a broad range of positive and negative q, the partition function $Z_q(a)$ scales as a power law (Fig. 2a, b).

For all healthy subjects, $\tau(q)$ is a nonlinear function (Figs 2c and 3a), which indicates that the heart rate of healthy humans is a multifractal signal. Figure 3b shows that, for healthy subjects, $D(h)$ has non-zero values for a broad range of local Hurst exponents h. The multifractality of healthy heartbeat dynamics cannot be explained by activity, as we analyse data from subjects at night. Furthermore, this multifractal behaviour cannot be attributed to sleep-stage transitions, as we find multifractal features during daytime hours as well. The range of scaling exponents ($0 < h < 0.3$) with non-zero fractal dimension $D(h)$ indicates that the fluctuations in the healthy heartbeat dynamics exhibit anti-correlated behaviour ($h = 1/2$ corresponds to uncorrelated behaviour; $h > 1/2$ corresponds to correlated behaviour).

In contrast, heart-rate data from subjects with a pathological

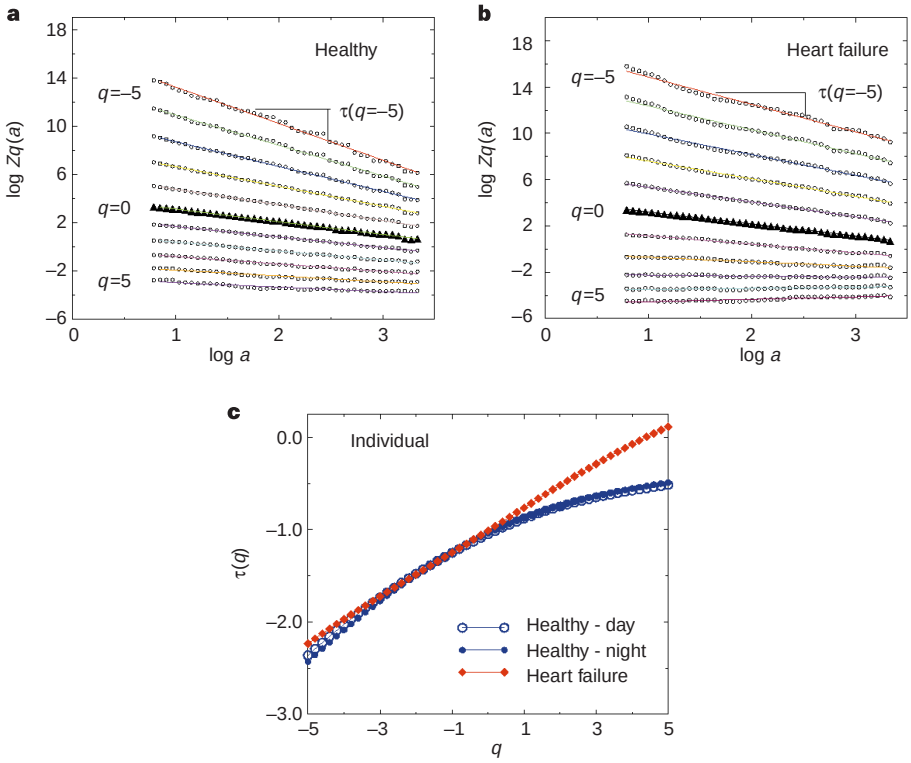

Figure 2 Heartbeat time series contain densely packed, non-isolated singularities which unavoidably affect each other in the time-frequency decomposition. Therefore, rather than evaluating the distribution of the inherently unstable local singularity exponents (as shown in Fig. 1), we estimate the scaling of an appropriately chosen global measure: the q moments of the probability distribution of the maxima of the wavelet transform $Z_q(a)$ (using the third derivative of the gaussian function as the analysing wavelet). The scaling of the partition function $Z_q(a)$ with scale a was obtained from daytime records consisting of ~25,000 beats for **a**, a healthy subject, and **b**, a subject with congestive heart failure. We calculate $\tau(q)$ for moments $q = -5, -4, \ldots 0, \ldots 5$ and scales $a = 2 \times 1.15^i$, $i = 0, \ldots 41$. We show the calculated values of $Z_q(a)$ for scales $a > 8$. Top curve $q = -5$; middle curve (bold), $q = 0$; bottom curve, $q = 5$. $\tau(q)$ are obtained from the slope of the curves in the region $16 < a < 700$, thus eliminating the influence of any residual small-scale random noise due to signal pre-processing as well as extreme, large-scale fluctuations of the signal. **c**, Multifractal spectrum $\tau(q)$ for individual records. A monofractal signal would correspond to a straight line for $\tau(q)$; for a multifractal signal $\tau(q)$ is nonlinear. Note the differences between the curves for healthy and heart-failure records. The changing curvature for the healthy records indicates multifractality. In contrast, $\tau(q)$ is linear for the subject with congestive heart failure, indicating monofractality.

condition—congestive heart failure—show a clear loss of multifractality (Fig. 3a, b). For the heart-failure subjects, $\tau(q)$ is close to linear and $D(h)$ is nonzero only over a very narrow range of exponents h, indicating monofractal behaviour (Fig. 3).

Our results show that, for healthy subjects, local Hurst exponents in the range $0.07 < h < 0.17$ are associated with fractal dimensions close to one. This means that the subsets characterized by these local exponents are statistically dominant. On the other hand, for the heart-failure subjects, the statistically dominant exponents are confined to a narrow range of local Hurst exponents centred at $h \simeq 0.22$. These results suggest that, for heart failure, the fluctuations are less anti-correlated than for healthy dynamics, as the dominant scaling exponents h are closer to 1/2.

We systematically compared our method with other widely used methods of heart-rate time-series analysis[12,21,22]. Several of these methods do not result in a fully consistent assignment of healthy

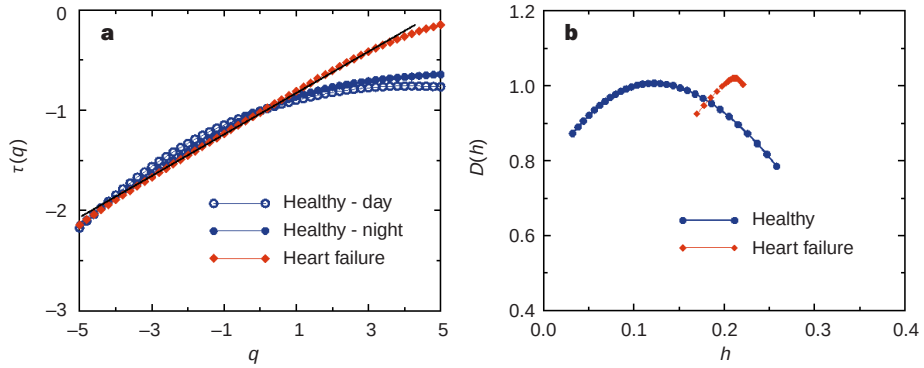

Figure 3 Multifractality in healthy dynamics. **a**, Multifractal spectrum $\tau(q)$ of the group averages for daytime and night-time records for 18 healthy subjects and 12 patients with congestive heart failure. The results show multifractal behaviour for the healthy group and different behaviour for the heart-failure group. **b**, Fractal dimensions $D(h)$ obtained through a Legendre transform from the group-averaged $\tau(q)$ spectra of **a**. The shape of $D(h)$ for the individual records and for the group average is broad, indicating multifractal behaviour. $D(h)$ for the heart-failure group is very narrow, indicating monofractality. The different form of $D(h)$ for the heart-failure group may reflect perturbation of the cardiac neuroautonomic control mechanisms associated with this pathology.

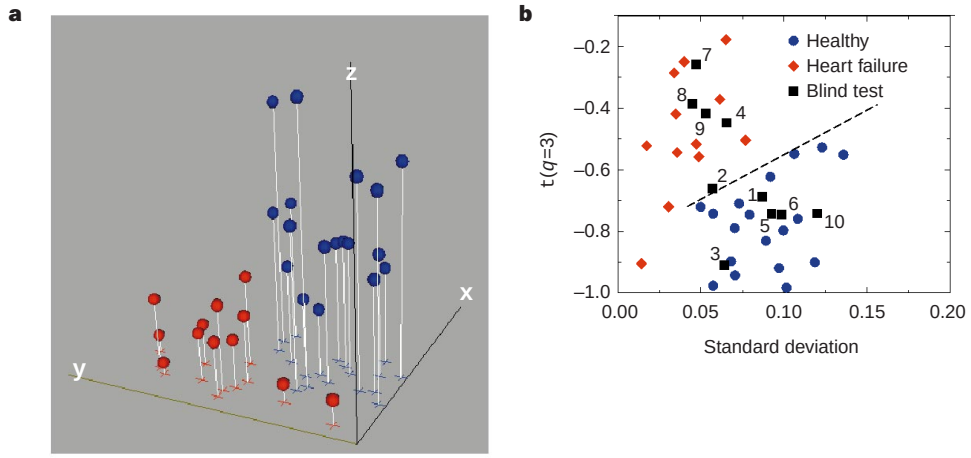

Figure 4 Discrimination method based on the multifractal formalism. **a**, Each subject's dataset in the database is characterized by three quantities. The first quantity (z-axis) is the degree of multifractality, which is the difference between the maximum and minimum values of local Hurst exponent h for each individual. The degree of multifractality is zero for a monofractal. The second quantity (y-axis) is the exponent value $\tau(q = 3)$ characterizing the scaling of the third moment, $Z_3(a)$. The third quantity (x-axis) is the standard deviation of the interbeat intervals. Blue spheres, healthy subjects; red spheres; heart-failure subjects. This multifractal approach discriminates healthy from heart-failure subjects. **b**, Discrimination method based on multifractal formalism for the 'blind' datasets. The y-axis is the exponent value $\tau(q = 3)$, and the x-axis is the standard deviation of the time series of interbeat intervals. Black squares show the results for the datasets of the blind test. Two of the heart-failure subjects (closest to the origin) do not fit as clearly in either group; however, they are clearly identified as unhealthy in **a** because their degree of multifractality (z-axis) is close to zero (these two subjects are indicated by the red spheres in **a** that are closest to the origin). These cases demonstrate that a single exponent is not sufficient to describe the complexity of a heartbeat time series.

versus diseased subjects (see http://polymer.bu.edu/~amaral/Heart.html). Figure 4a shows the results of our method based on the multifractal formalism. Each subject's dataset is characterized by three quantities: (1) the standard deviation of the interbeat intervals; (2) the exponent value $\tau(q = 3)$ obtained from the scaling of the third moment $Z_3(a)$; and (3) the degree of multifractality, defined as the difference between the maximum and minimum values of local Hurst exponent h for each individual (Fig. 5). The multifractal approach robustly discriminates healthy subjects from heart-failure subjects.

We next blindly analysed a separate database containing 10 records, 5 from healthy individuals and 5 from patients with congestive heart failure. The time series in the new database are shorter than those in our database; on average they are only 2-h long (less than 8,000 beats). Figure 4b shows the projection on the x–y plane of our data presented in Fig. 4a. The results for the blind test are shown in black. Our approach clearly separates the blind test subjects into two groups: 1, 3, 5, 6 and 10 fall in the healthy group, and 2, 4, 7, 8 and 9 in the heart-failure group. Unblinding the test code confirms these assignments. Thus, an analysis incorporating the multifractal method may add diagnostic power to contemporary analytic methods of heartbeat (and other physiological) time-series analysis.

The multifractality of heart-beat time series also enables us to quantify the greater complexity of the healthy dynamics compared to those of pathological conditions. Power-spectrum analysis defines the complexity of heart-beat dynamics through its scale-free behaviour, identifying a single scaling exponent as an index of healthy or pathological behaviour. Hence, the power spectrum cannot quantify the greater level of complexity of the healthy dynamics, reflected in the heterogeneity of the signal. In contrast, the multifractal analysis reveals this new level of complexity by the

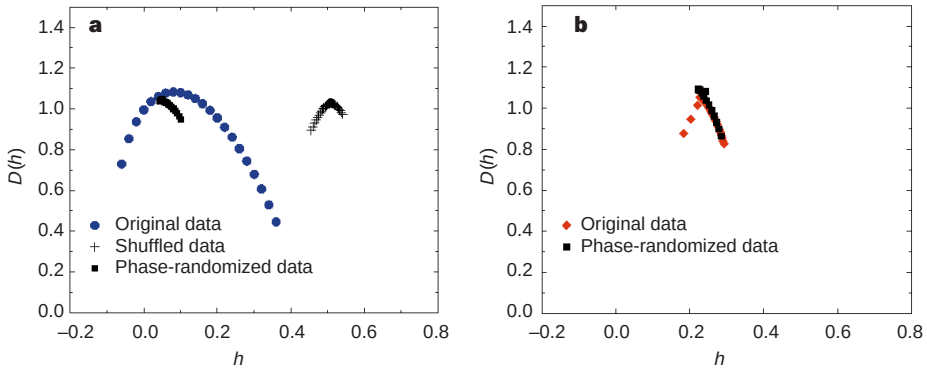

Figure 5 Nonlinearity and Fourier phases. **a**, The fractal dimensions $D(h)$ for a 6-h daytime record from a healthy subject. After reshuffling and integrating the increments in this interbeat-interval time series, so that all correlations are lost but the distribution is preserved, we obtain monofractal behaviour–a very narrow point-like spectrum centred at $h \equiv H = 1/2$. Such behaviour corresponds to a simple random walk. A different test, in which the $1/f$ scaling of the heartbeat signal is preserved but the Fourier phases are randomized (that is, nonlinearities are eliminated), leads again to a monofractal spectrum centred at $h \simeq 0.07$, because the linear correlations were preserved. These tests indicate that the multifractality is related to nonlinear features of the healthy heartbeat dynamics, rather than to the ordering or the distribution of the interbeat intervals in the time series. **b**, The fractal dimensions $D(h)$ for a 6-h daytime record from a heart-failure subject. The narrow multifractal spectrum indicates loss of multifractal complexity and reduction of nonlinearities with pathology.

broad range of exponents necessary to characterize the healthy dynamics. Moreover, the change in shape of the $D(h)$ curve for the heart-failure group may provide insight into the changes in the cardiac control mechanisms resulting from this pathology.

To study the complexity of the healthy dynamics further, we performed two tests with surrogate time series. First, we generated a surrogate time series by shuffling the interbeat interval increments of a record from a healthy subject. The new signal preserves the distribution of interbeat interval increments but destroys the long-range correlations among them. Hence, the signal is a simple random walk, which is characterized by a single Hurst exponent $H = 1/2$ and exhibits monofractal behaviour (Fig. 5a). Second, we generated a surrogate time series by performing a Fourier transform on a record from a healthy subject, preserving the amplitudes of the Fourier transform but randomizing the phases, and then performing an inverse Fourier transform. This procedure eliminates nonlinearities, preserving only the linear features of the original time series. The new surrogate signal has the same $1/f$ behaviour in the power spectrum as the original heart-beat time series; however, it exhibits monofractal behaviour (Fig. 5a). We repeated this test on a record from a heart-failure subject. In this case, there is a smaller change in the multifractal spectrum (Fig. 5b). The results suggest that the healthy heartbeat time series contains important phase correlations which are cancelled in the surrogate signal by the randomization of the Fourier phases, and that these correlations are weaker in heart-failure subjects. Furthermore, our analysis indicates that the observed multifractality is related to nonlinear features of the healthy heartbeat dynamics. Several studies have tested for nonlinear and deterministic properties in records of interbeat intervals[23–27]. We have demonstrated an explicit relation between the nonlinear features (represented by the Fourier phase interactions) and the multifractality of healthy cardiac dynamics (Fig. 5).

From a physiological perspective, the detection of robust multifractal scaling in the heart-rate dynamics is of interest because it indicates that the control mechanisms regulating the heartbeat might interact as part of a coupled cascade of feedback loops in a system operating far from equilibrium[28,29]. Furthermore, these results indicate that the healthy heartbeat is even more complex than previously suspected, posing a challenge to ongoing efforts to develop realistic models of the control of heart rate and other processes under neuroautonomic regulation. □

Methods

Heart failure (CHF) data were recorded using a Del Mar Avionics Model 445 Holter recorder and digitized at 250 Hz. Beats were labelled using 'Aristotle' arrhythmia analysis software, which labels each detected beat as normal, ventricular ectopic, supraventricular ectopic or unknown[30]. The location of the R-wave peaks is determined with a resolution of 4 ms.

Healthy datasets were recorded using a Marquette Electronics series 8500 Holter recorder. Using a Marquette Electronics model 8000T Holter scanner, the tapes were then digitized at 128 Hz, scanned and annotated. The annotations were manually verified by an experienced Holter scanning technician. The location of the R-wave peaks was thus determined with a resolution of 8 ms.

The finite resolution implies that our estimates of the interbeat intervals are affected by a white noise due to estimation error. The signal-to-noise ratio for both healthy and heart failure is of the order of 100. Furthermore, the white noise due to the measurements would lead to the detection of a local Hurst exponent $h = 0$ at very small scales. For that reason, we have considered only scales larger than 16 beats.

From the beat annotation file, only the intervals (*NN*) between consecutive normal beats were determined; thus intervals containing non-normal beats were eliminated from the *NN* interval series. For the CHF data, an average of 2% (range, 0.1 to 0.6%) of the intervals were eliminated, and for the normal data an average of 0.01% (range 0 to 0.06%) were eliminated. No interpolation was done for eliminated intervals.

To eliminate outliers due to missed beat detections which would give rise to erroneously large intervals that may have been included in the *NN* interval series, a moving-window average filter was applied. For each set of five contiguous *NN* intervals, a local mean was computed, excluding the central interval. If the value of the central interval was greater than twice the local average, it was considered to be an outlier and excluded from the *NN* interval series. This criterion was applied to each *NN* interval in the series. For the CHF data, an average of 0.02% (range 0 to 0.1%) of the intervals were eliminated, and for the normal data an average of 0.07% (range 0 to 0.7%) were eliminated. No interpolation was done for eliminated intervals. Overall a total of 2% (range, 0.1 to 6%) of the total number of *NN* intervals were eliminated for the CHF data and 0.08% (range 0 min to 0.7% max) for the normal data.

Next, we built a time series of increments between consecutive *NN* intervals and calculated their standard deviation. We then identified all pairs of associated increments with opposite signs and with an amplitude larger than 3 s.d. The values of the increments for each pair were replaced by linear interpolations of their values and the time series of *NN* interval time was reconstructed by integration from the filtered increments. About 1% of time intervals were corrected by this procedure.

Received 2 March; accepted 7 April 1999.

1. Bassingthwaighte, J. B., Liebovitch, L. S. & West, B. J. *Fractal Physiology* (Oxford Univ. Press, New York, 1994).
2. Dewey, T. G. *Fractals in Molecular Biophysics* (Oxford Univ. Press, Oxford, 1997).
3. Stanley, H. E. & Meakin, P. Multifractal phenomena in physics and chemistry. *Nature* **335,** 405–409 (1988).
4. Vicsek, T. *Fractal Growth Phenomena*, 2nd edn (World Scientific, Singapore, 1993).
5. Takayasu, H. *Fractals in the Physical Sciences* (Manchester Univ. Press, Manchester, UK, 1997).
6. Stanley, H. E. in *Fractals and Disordered Systems* 2nd edn (eds Bunde, A. & Havlin, S.) 1–68 (Springer, Berlin, 1996).
7. Shlesinger, M. F. Fractal time and 1/*f* noise in complex systems. *Ann. NY Acad. Sci.* **504,** 214–228 (1987).
8. Malik, M. & Camm, A. J. (eds) *Heart Rate Variability* (Futura, Armonk, NY, 1995).
9. Akselrod, S. *et al*. Power spectrum analysis of heart rate fluctuations: a quantitative probe of beat-to-beat cardiovascular control. *Science* **213,** 220–222 (1981).
10. Kobayashi, M. & Musha, T. 1/*f* fluctuation of heartbeat period. *IEEE Trans. Biomed. Eng.* **29,** 456–457 (1982).
11. Hausdorff, J. M. *et al*. Fractal dynamics of human gait: stability of long-range correlations in stride interval fluctuations. *J. Appl. Physiol.* **80,** 1448–1457 (1996).
12. Peng, C.-K., Havlin, S., Stanley, H. E. & Goldberger, A. L. Quantification of scaling exponents and crossover phenomena in nonstationary time series. *Chaos* **5,** 82–87 (1995).
13. Hurst, H. E. Long-term storage capacity of reservoirs. *Trans. Am. Soc. Civ. Eng.* **116,** 770–808 (1951).
14. Vicsek, T. & Barabási, A. L. Multi-affine model for the velocity distribution in fully turbulent flows. *J. Phys. A* **24,** L845–L851 (1991).
15. Barabasi, A.-L. & Stanley, H. E. *Fractal Concepts in Surface Growth* Ch. 24 (Cambridge Univ. Press, Cambridge, 1995).
16. Daubechies, I. *Ten Lectures on Wavelets* (SIAM, Philadelphia, 1992).
17. Ivanov, P. Ch. *et al*. Scaling behaviour of heartbeat intervals obtained by wavelet-based time-series analysis. *Nature* **383,** 323–327 (1996).
18. Muzy, J. F., Bacry, E. & Arneodo, A. Wavelets and multifractal formalism for singular signals: application to turbulence data. *Phys. Rev. Lett.* **67,** 3515–3518 (1991).
19. Muzy, J. F., Bacry, E. & Arneodo, A. The multifractal formalism revisited with wavelets. *Int. J. Bifurc. Chaos* **4,** 245–302 (1994).
20. Peng, C.-K. *et al*. Fractal mechanisms and heart rate dynamics: Long-range correlations and their breakdown with disease. *J. Electrocardiol.* **28,** 59–65 (1996).
21. Thurner, S., Feurstein, M. C. & Teich, M. C. Multiresolution wavelet analysis of heartbeat intervals discriminates healthy patients from those with cardiac pathology. *Phys. Rev. Lett.* **80,** 1544–2391 (1998).
22. Amaral, L. A. N., Goldberger, A. L., Ivanov, P. Ch. & Stanley, H. E. Scale-independent measures and pathologic cardiac dynamics. *Phys. Rev. Lett.* **81,** 2388–2391 (1998).
23. Lefebvre, J. *et al*. Predictability of normal heart rhythms and deterministic chaos. *Chaos* **3,** 267–276 (1993).
24. Yamamoto, Y. *et al*. Operation Everest II: an indication of deterministic chaos in human heart rate variability at simulated extreme altitude. *Biol. Cybern.* **69,** 205–212 (1993).
25. Kanters, J. K., Holstein-Rathlou, N. H. & Agner, E. Lack of evidence for low-dimensional chaos in heart rate variability. *J. Cardiovasc. Electrophysiol.* **5,** 128–137 (1994).
26. Sugihara, G., Allan, W., Sobel, D. & Allan, K. D. Nonlinear control of heart rate variability in human infants. *Proc. Natl Acad. Sci. USA* **93,** 2608–2613 (1996).
27. Poon, C-S. & Merrill, C. K. Decrease of cardiac chaos in congestive heart failure. *Nature* **389,** 492–495 (1997).
28. Meneveau, C. & Sreenivasan, K. R. Simple multifractal cascade model for fully developed turbulence. *Phys. Rev. Lett.* **59,** 1424–1427 (1987).
29. Ivanov, P. Ch., Amaral, A. L. N., Goldberger, A. L. & Stanley, H. E. Stochastic feedback and the regulation of biological rhythms. *Europhys. Lett.* **43,** 363–368 (1998).
30. Moody, G. B. & Mark, R. G. Development and evaluation of a 2-lead ECG analysis program. *Computers Cardiol.* **9,** 39–44 (1983).

Acknowledgements. We thank A. Bunde, U. Frisch, J. M. Hausdorff, V. Horváth, H. Kallabis, R. G. Mark, J. Mietus, C.-K. Peng, K. R. Sreenivasan and B. J. West for discussions. We are especially grateful to A. Arneodo and T. Vicsek for advice on the analytical technique and on the text and R. Goldsmith for providing the blind test data. This work was supported by NASA, NIH, FCT/Portugal, and The G. Harold and Leila Y. Mathers Charitable Foundation.

Correspondence and requests for materials should be addressed to P.Ch.I. (e-mail: plamen@buphy.bu.edu